Title
Control of hierarchical polymer mechanics with bioinspired metal-coordination dynamics.

Journal
Nature materials, 14(12)

ISSN
1476-1122

Authors
Grindy, Scott C
Learsch, Robert
Mozhdehi, Davoud
et al.

Publication Date
2015-12-01

DOI
10.1038/nmat4401

Peer reviewed

HHS Public Access

Author manuscript

Nat Mater. Author manuscript; available in PMC 2016 May 18.

Published in final edited form as:

Nat Mater. 2015 December ; 14(12): 1210–1216. doi:10.1038/nmat4401.

Control of hierarchical polymer mechanics with bioinspired metal-coordination dynamics

Scott C. Grindy[1], **Robert Learsch**[1], **Davoud Mozhdehi**[3], **Jing Cheng**[2], **Devin G. Barrett**[2], **Zhibin Guan**[3], **Phillip B. Messersmith**[2,*], and **Niels Holten-Andersen**[1,†]

[1]Department of Materials Science and Engineering, Massachusetts Institute of Technology, Cambridge, Massachusetts 02139

[2]Department of Biomedical Engineering, Northwestern University, Evanston, Illinois 60208

[3]Department of Chemistry, University of California, Irvine, California 92697

Abstract

In conventional polymer materials, mechanical performance is traditionally engineered via material structure, using motifs such as polymer molecular weight, polymer branching, or copolymer-block design[1]. Here, by means of a model system of 4-arm poly(ethylene glycol) hydrogels crosslinked with multiple, kinetically distinct dynamic metal-ligand coordinate complexes, we show that polymer materials with decoupled spatial structure and mechanical performance can be designed. By tuning the relative concentration of two types of metal-ligand crosslinks, we demonstrate control over the material's mechanical hierarchy of energy-dissipating modes under dynamic mechanical loading, and therefore the ability to engineer *a priori* the viscoelastic properties of these materials by controlling the types of crosslinks rather than by modifying the polymer itself. This strategy to decouple material mechanics from structure may inform the design of soft materials for use in complex mechanical environments.

Soft materials are often utilized to engineer interfaces in complex environments. For example, hydrogels are currently explored in a variety of biomedical applications including synthetic cartilage, subcutaneous drug delivery, biomechanical actuators, tissue scaffolds, and injectable wound-healing materials[2,3]. Many of these applications involve considerable mechanical loads of both static and dynamic character and much current research is focused on identifying strategies for enhancing the strength, stiffness, and toughness of hydrogels and other soft polymer materials[4–9]. Using spatial design elements such as double-network structures, hard secondary inorganic phases, or self-assembled nanostructures, most of these strategies are geared toward control over the spatial structure of the polymer networks across multiple hierarchical length scales. However, there is an additional dimension of scale that cannot be overlooked when designing soft matter systems: time. Soft materials often possess critical structural motifs that operate at multiple hierarchical time scales in addition to

†Corresponding author: ; Email: holten@mit.edu

*Current affiliation: Departments of Bioengineering and Materials Science and Engineering, University of California, Berkeley, California 94720

multiple hierarchical length scales. Kinetic effects can therefore dominate the mechanical response, and a material that is quite tough or strong at one strain rate may be brittle or weak at another. Yet, studies of the relevant time scales of soft material mechanics are typically limited to characterization rather than design. This is primarily due to the inherent coupling between the spatial and temporal structure of the material, where spatial structural motifs directly determine the associated time scales. For example, the molecular weight and persistence length of a polymer (spatial structure) directly determine its reptation time (temporal structure)[10].

In contrast to the traditional focus on material spatial hierarchy, we propose to instead specifically engineer polymer material temporal hierarchy *orthogonally* from the spatial hierarchy. Hence, the goal of our study is to de-couple spatial and temporal polymer material hierarchies such that we can use motifs from both dimensions as orthogonal mechanical design elements (see Figure 1). To do this we employ nearly-ideal hydrogel network polymers crosslinked with metal-coordinate bonds inspired by the self-healing, tough, and strong fibers that mussels use to adhere to underwater substrates[11,12]. These types of crosslinks are typically reversible, such that when used as the defining mechanical crosslink in hydrogel systems the mechanical properties are primarily dictated by the metal-ligand exchange kinetics[13,14]. These kinetics can vary across several orders of magnitude in time by the choice of ligand and metal ion[15–20]. Recently, researchers have identified dynamic interactions (such as metal-ligand coordination) as a way to create tough hydrogels[4–6,21] or mimic natural tissue mechanical properties[22]. As such, there is considerable current development in the theories of mechanical behavior of transient networks.[23–25]

We show here that by evenly mixing multiple kinetically distinct metal-ligand crosslinks within the same hydrogel network we obtain explicit control over hierarchical mechanical properties across several orders of magnitude in time, independent of the polymer network spatial hierarchy. De-coupling of the network mechanical timescales from the polymer structural length scales shows a new paradigm for spatial structure-independent viscoelastic materials design. We show how we control mechanical temporal hierarchy in two ways: (1) using a model system where the interpretation is straightforward and quantitative, and (2) we extend our treatment to less-ideal systems to show the generality of our approach of de-coupling structure from function. Figure 1 schematically illustrates this concept.

Our model system is composed of an aqueous solution of 4-arm polyethylene glycol polymers where the end of each arm is functionalized with a histidine moiety (Figure 1, 4PEG-His). By mixing the 4PEG-His with divalent transition metal ions and increasing the pH, His_2-M^{2+} complexes form and act as crosslinks in viscoelastic gel networks. To study the time-dependent mechanical properties of these gels we use oscillatory strain rheometry, which measures the storage ($G'(\omega)$) and loss ($G''(\omega)$) viscoelastic moduli at different frequencies of oscillating strain (see Figure 2a). The reciprocal of the critical frequency ω_c where $G'(\omega) = G''(\omega)$ is called the materials characteristic relaxation time, denoted τ_c. At frequencies above $1/\tau_c$, the material elastically stores more energy than it dissipates ($G'(\omega) > G''(\omega)$, solid-like behavior), while at frequencies below $1/\tau_c$, the material dissipates more energy than it stores ($G''(\omega) > G'(\omega)$, fluid-like behavior). Hence, the molecular relaxation

mechanisms that control τ_c dictate the energy-storing and energy-dissipating properties of a soft material under dynamic mechanical loading.

At frequencies below $1/\tau_c$, the visco-elastic moduli are expected to follow the scaling relations for terminal relaxation: $G'(\omega) \sim \omega^2$ and $G''(\omega) \sim \omega^1$. As reported by Fullenkamp *et al*[15], when His-Ni^{2+}, His-Cu^{2+}, or His-Zn^{2+} complexes are used as the unique crosslinks of 4PEG-His hydrogel networks we indeed observe this scaling behavior (see Figure 2a) and we observe the relaxation times $\tau_{Ni} \sim 10^1 s > \tau_{Cu} \sim 10^{-2} - 10^- s \gg \tau_{Zn}$. The identification of a single characteristic relaxation timescale represents a naive first approximation of the material temporal structure of single metal-ion hydrogels. However, we can quantify the full distribution of relaxation times by converting the experimentally-measured storage and loss moduli into a distinct material function of relaxation times called the relaxation spectrum, $H(\tau)$, by solving the following integral equations:

$$G'(\omega) = \int_{-\infty}^{\infty} H(\tau) \frac{\omega^2 \tau^2}{1+\omega^2 \tau^2} dln(\tau) \quad (1a)$$

$$G''(\omega) = \int_{-\infty}^{\infty} H(\tau) \frac{\omega \tau}{1+\omega^2 \tau^2} dln(\tau) \quad (1b)$$

$H(\tau)$ has units of Pascals and is equivalent to an infinite parallel series of Maxwell elements (a spring in series with a dashpot) along the time axis[26]. Each Maxwell element may be thought of as a characteristic strain energy-dissipating molecular relaxation mode within the material, with a resonant frequency given by $1/\tau$, the inverse of its individual relaxation time. Figures 2b and c schematically illustrate this concept and Figure 2d shows how the fitted relaxation spectrum correlates with the experimental $G'(\omega)$ and $G''(\omega)$ for the single metal-ion His-Ni^{2+} gel. The physical meaning of the relaxation spectrum is best understood in terms of energy storage and dissipation: the amount of energy dissipated under dynamic loading at frequency ω is proportional to $H(1/\omega)$, while the amount of energy stored is proportional to the cumulative integral $\int_{-\infty}^{1/\omega} H(\tau) dln(\tau)$.

By controlling one material dissipation mode, single metal-ion hydrogels thereby allow us to engineer one level in the material temporal hierarchy. However, we seek to gain multi-scale control over molecular relaxation times and thereby multi-level control over mechanical hierarchical dissipation. To achieve this goal we established hydrogel networks with two different His-M^{2+} complex crosslinks: Ni^{2+}:Zn^{2+} and Ni^{2+}:Cu^{2+} (see Figure 3). These double metal-coordinate networks indeed display two mechanically distinct relaxations: one slow dissipation mode at $\omega \sim 10^{-2} - 10^0$ rad/s ($\tau \sim$ 100–1 s) and one fast mode at $\omega \sim 10^1 - 10^2$ rad/s ($\tau \sim$ 0.1–0.01 s) as evinced by the double-peak form of $G''(\omega)$ in Figure 3. To explore our level of control over these hierarchical mechanical relaxation modes a series of gels were made with a constant total metal concentration at a stoichiometric 2:1 His:M^{2+} ratio, but where the ratio of either Zn^{2+}:Ni^{2+} or Cu^{2+}:Ni^{2+} was varied. As shown in Figure 2a, His-Ni^{2+} single metal-ion gels have long relaxation times while His-Cu^{2+} and His-Zn^{2+}

single metal-ion gels relax much faster and as such, each double-metal network should contain controllable concentrations of slow His-Ni^{2+} crosslinks and fast His-Zn^{2+} or His-Cu^{2+} crosslinks (see Figure 1). By calculating the relaxation spectra $H(\tau)$ for a series of gels with varying ratios of slow and fast crosslinks we can quantify not only the timescales but also the magnitudes of these metal-coordinate molecular dissipation modes and thereby estimate our level of control over the temporal hierarchy of our model system.

The observed two-peak forms of $G''(\omega)$ in Figure 3 suggests corresponding two-peak forms of $H(\tau)$ and we estimate the form of the relaxation spectrum as a two-mode log-normal distribution of relaxation times[27–29]:

$$H(\tau)=A_{slow}\exp\left(-\frac{(ln(\tau)-ln(\tau_{slow}))^2}{2\sigma_{slow}^2}\right)+A_{fast}\exp\left(-\frac{(ln(\tau)-ln(\tau_{fast}))^2}{2\sigma_{fast}^2}\right) \quad (2)$$

where each relaxation mode is distributed log-normally with amplitude A_i and standard deviation σ_i along the time axis (see the Methods section for details on the fitting procedure). We can fit the multi-peak relaxation spectrum $H(\tau)$ to the experimental storage ($G'(\omega)$) and loss ($G''(\omega)$) moduli data well (Figure 3, fit lines superimposed on top of $G'(\omega)$ and $G''(\omega)$ data; $H(\tau)$ is shown as a function of $1/\tau$ in the lower plot of each figure).

As Figure 3 shows, metal ion composition allows multi-scale control over dissipation modes in the mechanical hierarchy of double metal-coordinate network gels. At high concentrations of Ni^{2+} (Figure 3a and b, left), the slow dissipation mode has a much larger magnitude than the fast mode, and therefore dominates the mechanical hierarchy of the gel. As the concentration of Ni^{2+} in the gel decreases relative to the Zn^{2+} or Cu^{2+} concentration, the low frequency dissipation peak decreases in size while the high frequency peak increases, strongly suggesting that His-Ni^{2+} crosslinks are responsible for the slow dissipation mode while His-Zn^{2+}/Cu^{2+} crosslinks are responsible for the fast dissipation mode. These tunable bulk dissipative properties are similar to the behavior observed when changing the fraction of two phases in macroscopic composite materials, except that our gels are not macroscopic composites but molecular-scale hybrid networks.

To better examine the network-coupled metal-coordinate complex dissipation mechanisms we quantify the magnitude of the i^{th} (slow or fast) dissipation mode by the area under its corresponding peak, $P_i \equiv \int_{-\infty}^{\infty} A_i \exp\left(-\frac{ln(\tau)-ln(\tau_i)^2}{2\sigma_i^2}\right) dln(\tau) = A_i\sigma_i\sqrt{2\pi}$ using the conventions of Equation 3 and define the *relative contribution* of each dissipation mode as $P_i/\Sigma P_i$. These data are summarized in Figure 4.

While the mixed metal ion composition of our hydrogels directly modulates the relative contributions of the fast and slow dissipation modes, the relationships are non-linear and of opposite trend in Ni^{2+}:Cu^{2+} *vs.* Ni^{2+}:Zn^{2+} compositions; the relative contribution of the slow relaxation mode (associated with His-Ni^{2+} complexes) dominates the fast mode in Ni^{2+}:Zn^{2+} gels (Figure 4, top) but is dominated by the fast relaxation mode in Ni^{2+}:Cu^{2+} gels (Figure 4, bottom). Differences in histidine affinity is one plausible mechanism that

may explain this behavior: past work[15,30] suggests that histidine affinity for the metal ions follows the order $Cu^{2+} > Ni^{2+} > Zn^{2+}$ which would account for the different abilities of Zn^{2+} and Cu^{2+} to control energy dissipation modes within the network. While the precise mechanism is unknown at this time the tunability of the distinct relaxation modes within these networks suggests that metal-histidine complexes are excellent candidates for controlling multimodal energy dissipation within materials.

To emphasize how our approach differs from previous attempts to control time-dependent mechanical properties, it is useful to consider work by Annable *et al*[31] that focused on modulating the mechanical properties of hydrogel systems by using telechelic hydrophilic polymers with hydrophobic end-caps. They found that by changing the length of the hydrophobic end-cap different material relaxation times could be engineered, and further that mixtures of polymers with different end-cap lengths gave viscoelastic properties with multiple distinct relaxation times, in an analogous manner to our hybrid gels containing multiple metal ions. While the tunability of the macroscopic time-dependent mechanical properties is quite similar between the two systems, the important difference lies in the uncoupling of viscoelastic properties from macromolecular structure in our metal-coordinate polymer system: we are able to control the time-dependent mechanical properties orthogonally from the polymer structure simply with the choice of metal ions at the crosslink centers.

To show the generality and applicability of our approach, we conducted mechanical tests on three similar but distinct systems, all of which show the effects of temporal hierarchy to varying degrees. First, we showed the independence of our approach by showing that hydrogels crosslinked with one metal ion and two different ligands also shows temporally hierarchal mechanical behavior (Figure 5). 3,4 dihydroxyphenylalanine (dopa), another mussel-inspired modified amino acid known to strongly coordinate transition metals, also coordinates Ni^{2+} [32] and therefore we made 4PEG gels crosslinked with both dopa:Ni^{2+} and His:Ni^{2+} complexes. The rheological data shows that $G''(\omega)$ has two local maxima, indicative of two distinct relaxation timescales (Figure 5a). In an analagous manner to our gels crosslinked with His and two divalent metal ions, the magnitude of the slow relaxation mode is proportional to the concentration of 4PEG-His, while the magnitude of the fast relaxation mode increases as the concentration of 4PEG-dopa increases.

Second, we synthesized hydrogels that contain permanent covalent bonds in addition to dynamic His-metal ion associations to show that metal-coordinate complexes can be added to conventional hydrogels to control temporal hierarchy. To form these hydrogels, we added 4PEG-N-Hydroxysuccinimide (4PEG-NHS) and 4PEG-NH_2 to solutions of 4PEG-His, thereby creating solid hydrogels via covalent amide linkages while leaving free HIs groups for His:Ni^{2+} dynamic crosslinks. While these covalent/dynamic hydrogels at pH 5.2 show no discernible characteristic energy dissipation during rheological tests, at pH 7.4 the hydrogels show distinct energy dissipation peaks at similar frequencies to the characteristic timescale of 4PEG-His:Ni^{2+} hydrogels (Figure 5b). Upon reducing the pH of the hydrogel back to pH 5.2, the resonant energy dissipation peak disappears. This demonstration confirms that His:Ni^{2+} metal-coordinate bonds are modular energy-dissipating motifs that can be inserted

into less ideal networks and retain their ability to control the temporal mechanical hierarchy of materials.

Finally, we wanted to further show the generality of our approach by demonstrating that we can control temporal hierarchy outside of the hydrogel material space. To do this we synthesized a linear imidazole-containing copolymer (L-ICP) by copolymerizing n-butyl acrylate and a previously reported imidazole acrylate monomer (IMZa) (Figure 5c)[9]. Melt-like polymer materials were created by mixing L-ICP and metal salts at an 8:1 imidazole:M^{2+} and evaporating the solvent. Three separate samples were prepared, using Ni^{2+}, Cu^{2+}, and a 50/50 mixture of Ni^{2+} and Cu^{2+}. Under rheological testing, the dynamic viscosity $|\eta^*|$ of each melt shows qualitatively similar behavior: a low-frequency Newtonian regime where $|\eta^*| \sim \omega^0$, and a shear-thinning regime where $|\eta^*| \sim \omega^{-1/3}$. However, the frequency at which each melt transitions from the Newtonian to shear-thinning regimes (the inverse of the material's terminal relaxation time) is distinct for each of the three materials tested, and follows the order $\omega_{Ni} < \omega_{50/50} < \omega_{Cu}$ (Figure 5c). Thus, by choosing a melt system vastly different from our model hydrogel systems (solvent-free melt vs. water-swollen hydrogel, imidazole vs. histidine coordinating ligand, and 8:1 vs. 2:1 ligand:metal stoichiometry), these data suggest that imidazole-based metal coordination can also be used outside of hydrogel systems to control materials' mechanical temporal hierarchy.

The remarkable structural hierarchy displayed in nature's materials is now well documented, yet the possible evolution of an orthogonal temporal hierarchy in biomaterials has to our knowledge never been investigated. We hope that our demonstration of complex material behavior of simple bio-inspired metal-coordinate model gels will not only prove useful in synthetic polymer materials engineering but also provide future inspiration for integrated spatio-temporal studies of nature's hierarchical material designs. Insights from such studies would not only advance our understanding of biological materials evolution, but also expand the functional property space of soft materials by uncovering a new source of ideas for bio-inspired mechanical engineering.

Methods

Synthesis of 4PEG-His

4PEG-His was synthesized in the manner of Ref. [15]. Briefly: 5 g of 10kDa 4-arm PEG-NH_2 was mixed with 1.49 g Boc-His(Trt)-OH and 1.33 g BOP reagent and dissolved in 15 mL dichloromethane. 1.07 mL DIPEA was added and the reaction was allowed to proceed for 2 hours. The product was purified by precipitation in 500 mL diethyl ether 1x, 500 mL methanol at −20°C 3x, diethyl ether 1x, then vacuum dried. Protecting groups were removed by a cleavage solution of 95 mL trifluoroacetic acid, 2.5 mL triisopropylsilane, and 2.5 mL water for 2 hours. The solvent was removed under reduced pressure and the product purified by re-dissolving in methanol, precipitation in ether 3x, and vacuum drying.

Synthesis of 4PEG-DOPA

Conversion of 4PEG-OH to 4PEG-COOH—To a 1-L round bottom flask, 25 g of 4-arm PEG (20 kDa) and 600 mL H_2O were added and stirred. Once the PEG had dissolved, 200

mg TEMPO and 200 mg NaBr were added. After a homogenous solution was formed, 50 mL of aqueous NaClO (10–15% available chlorine) was added. While continuously monitoring the pH, the solution was stirred for 30 min. The pH was maintained between 10 and 11 with 1 M NaOH. To halt the reaction, 50 mL of ethanol was added, and the pH was decreased to 2 with 12.1 M HCl (Note: Be extremely careful with such strong acid). The aqueous mixture was extracted with 4 portions of 150–200 mL dichloromethane. The combined organic layers were extracted with 700 mL MilliQ H2O and dried with MgSO4. After filtering, the DCM was removed by rotary evaporation. The crude 4-arm PEG-COOH was purified by precipitating in −20°C methanol, freezing at −80°C, and drying under vacuum for 24 h. Any 4PEG-COOH not immediately used was stored at −20°C.

Conversion of 4PEG-COOH to 4PEG-dopa—In a 250-mL round bottom flask, 10 g 4PEG-COOH, 50 mL DMF, and 25 mL of CH_2Cl_2 were mixed until the PEG completely dissolved. Dopamine (1.2x mol eq relative to -COOH) and HBTU (1.2x mol eq relative to -COOH) were sequentially added and mixed until completely dissolved. Triethylamine (2.2x mol eq relative to -COOH) was added to start the reaction, which proceeded at room temperature for 2 h. The reaction solution was reduced via rotary evaporation to remove the DCM. The crude 4PEG-dopa was purified by precipitation in acidified diethyl ether and acidified methanol. The PEG was then dialyzed (3500 MWCO) in pH 3.5 MilliQ H_2O for 24 h and in unadjusted MilliQ H_2O for 2 h. The aqueous solution was frozen at −80°C and lyophilized for 3 days. The final 4PEG-dopa was stored at −20°C.

Synthesis of 4PEG-His:M^{2+} and 4PEG-DOPA:M^{2+} Hydrogels

A 200 mg/mL aqueous solution of 4PEG-His + 4PEG-DOPA in the desired proportion was mixed with 0.1 M $NiCl_2 \cdot 6H_2O$, $CuCl_2 \cdot 6H_2O$, or $ZnCl_2$ such that the ([His] + [DOPA]): $[M^{2+}]_{total}$ ratio was fixed at 2:1. De-ionized water was added such that the final concentration of the gel would be 100 mg/mL, and 1 M NaOH was added to induce gelation in a NaOH:([His] + [DOPA]) ratio of 2:1.

Rheometric Measurements of 4PEG-His:M^{2+} and 4PEG-His:4PEG-dopa:M^{2+} Hydrogels

All mechanical properties were measured on an Anton Paar MCR 302 rheometer in either a 25 mm diameter cone-plate geometry with a 51 μm truncation and a 1° cone angle or a 10 mm diameter plate-plate geometry at a temperature of 5°C. A layer of mineral oil was used to block solvent evaporation. Frequency sweeps were performed by applying a sinusoidal strain, $\gamma = \gamma_0 sin(\omega t)$, with γ_0 = 1%, well within the linear viscoelastic range (see Figures S1–S3).

Synthesis of 4PEG-NHS:4PEG-NH_2:4PEG-His:M^{2+} Hydrogels

4PEG-His was synthesized as described above. 4PEG-Amine Hydrochloride (4PEG-NH_2) and 4PEG-Succinimidyl Glutaramide (4PEG-NHS) (MW = 10,000 g/mol) were purchased from JenKem Technology USA and used as received. 4PEG-NH_2 and 4PEG-His were dissolved in 0.1M phosphate buffer, pH 7.4 (Sigma-Aldrich), and 4PEG-NHS was dissolved in 0.1M Sodium Acetate buffer (Sigma-Aldrich), at concentrations targeting the final composition of the hydrogel: 0.01M for 4PEG-NHS and 4PEG-NH_2 and 0.005M for 4PEG-His for the data shown in Figure 5b. The solutions were then mixed in equal volumes (1/3 of

the unswollen volume of the cured hydrogel) and poured into a mold, sealed to prevent evaporation and cured for at least 4 hours as an adaptation of the procedure of Sakai *et al*[33]. The resulting solid hydrogel was rinsed in MilliQ H_2O, then soaked in excess 0.1M $NiCl_2$.6H2O in MilliQ H_2O and pH 7.4 0.5M phosphate buffer for 4 hours each. Samples were stored in humidified environments until they could be sectioned and tested. Buffer exchanges were performed by rinsing the solid gels in excess 0.5M Sodium Acetate buffer, pH 5.2 for at least 4 hours.

Rheometric Measurements of 4PEG-NHS:4PEG-NH_2:4PEG-His:M^{2+} Hydrogels

Hydrogels were sectioned with a razor blade to cut them down to the appropriate size for rheometric tests. Hydrogels were measured on an Anton Paar MCR 302 rheometer in a 10 mm diameter plate-plate geometry at a temperature of 25°C. A conventional solvent trap was used to block solvent evaporation. Frequency sweeps were performed by applying a sinusoidal strain, $\gamma = \gamma_0 sin(\omega\tau)$, with $\gamma_0 = 0.1\%$, well within the linear viscoelastic range.

Synthesis of Linear Imidazole-Containing Polymer Melts

A linear imidazole containing copolymer (L-ICP) was synthesized by copolymerization of n-butyl acrylate (BA) and previously reported imidazole acrylate monomer (IMZa)[9] in the presence of small molecule chain transfer agent using RAFT living/controlled polymerization (Scheme S1).

IMZa (9.8 g, 35 mmol), BA (9.3 mL, 65 mmol), 1 mL anisole as NMR internal standard were dissolved in DMF (58 mL, 1.5 M with respect to vinyl moiety) and added to a Schlenk flask. Benzyl ethyl carbonotrithioate, chain transfer agent, (9 mg, 0.4 mmol) and AIBN (20 mg, 0.12 mmol) were then added to the reaction flask to prepare the reaction mixture with the following ratios: [Monomer]:[CTA]:[AIBN] = 250:1:0.2. The flask was sealed by a rubber septum and the mixture was purged with a stream of N_2 for 45 min. After which, the schlenk flask was immersed in an oil bath thermostatted at 65°C. After 150 min, the reaction was removed from the oil bath and was cooled on ice. After monitoring the conversion with ^{1}H NMR, 10 mg of 4-methoxyphenol was added as radical inhibitor and the reaction mixture was evaporated *in vacuo*. The residue was transferred to Nalgene centrifuge tubes and the polymer was precipitated in Et_2O/Hexane mixture, (1:3 v/v) followed by centrifugation at 8500 rpm, for 10 min at 4°C. The supernatant was decanted and the polymer was dissolved in CH_3CN and precipitated three more times in Et_2O/Hexane (4:1 v/v).

Average degree of polymerization ≈ 115 (determined by monitoring ^{1}H NMR conversion of monomers), 35% IMZa (mol %, determined by ^{1}H NMR analysis of purified polymer). M_n = 5.4 kg/mol, M_w/M_n = 1.4 (GPC, DMF as eluent, PEG as standard).

The polymer was then dissolved in CH_3CN and the stock solution was kept at 4°C. The concentration of polymer (mg/mL) was determined by gravimetric analysis. After determination of the imidazole content of each polymer sample using ^{1}H NMR, a stock solution of polymers were prepared in CH_3CN. Bis(trifluoromethane)sulfonimide salts, $M(NTf_2)_2$ where M is copper or nickel ($Ni(NTf_2)_2$ was purchased from Alfa Aesar; $Cu(NTf_2)_2$ from Sigma-Aldrich) were dissolved in CH_3CN and added incrementally to the

polymer solutions. After the complete addition of metal, the clear colored solutions were poured into a Teflon dish. The solvent was removed by heating the samples in a vacuum oven overnight at 80°C. The resulting coordinatively cross-linked polymers were scraped or collected from the Teflon dish and stored in a desiccator for further studies.

Rheometric Measurements of L-ICP Melts

Melt rheology was measured on an Anton-Paar MCR 302 rheometer in a 25 mm diameter parallel-plate geometry. Frequency sweeps were performed from ω = 100 rad/s to 0.1 rad/s at T = 80, 70, 60, 50, 40, 30, and 20°C at γ_0 = 1%. Master curves were generated using the time-temperature superposition algorithm of Bae *et al*, Ref. [34].

Calculating the Relaxation Spectrum $H(\tau)$

Relaxation spectra were calculated from frequency sweep data using a nonlinear iterative optimization algorithm using the matlab® function *lsqcurvefit*. The algorithm acted to minimize the following expression over the coefficients from the double log-normal relaxation spectrum A_{slow}, τ_{slow}, σ_{slow}, A_{fast}, τ_{fast}, and σ_{fast} (Equation 2):

$$\min_{\{coeffs\}} \sum_{\omega_i} \{\log_{10}(G'_{fit}(\omega_i)) - \log_{10}(G'_{data}(\omega_i))\}^2 + \{\log_{10}(G''_{fit}(\omega_i)) - \log_{10}(G''_{data}(\omega_i))\}^2 \quad (3)$$

Where G^n_{fit} is the storage or loss modulus calculated using Equations 2 and 3, and G^n_{data} is the experimentally measured data. In effect, the algorithm is acting to minimize the logarithmically-weighted sum of squares between the calculated and experimental data. For nonlinear fitting procedures, initial guesses of the parameters and lower and upper bounds must be set. Initial guesses for A_i, τ_i, and σ_i were set at $max(G')/2$ Pa, at $\omega(G''_{localmax})^{-1}$ s, and at 0.1 log(s), respectively. Lower and upper bounds for A_i, τ_i, and σ_i were set at (0 Pa, 2 × 10^5 Pa), ($max(\omega)^{-1}$ s, $min(\omega)^{-1}$ s), and (0 log(s), 10 log(s)) respectively.

Supplementary Material

Refer to Web version on PubMed Central for supplementary material.

Acknowledgments

SCG was supported by the Anne M. Mayes Fellowship. SCG and NHA were supported by the MRSEC program of the National Science Foundation under award number DMR - 0819762. NHA was supported by the MIT Sea Grant via the Doherty Professorship in Ocean Utilization. DGB, JC, and PBM were supported by the National Institutes of Health under award number R37DE014193. DM and ZG were supported by the US Department of Energy, Division of Materials Sciences, under award number DE-FG02-04ER46162.

References

1. Shaw, MT.; MacKnight, WJ. Introduction to Polymer Viscoelasticity. 3. Wiley-Interscience; 2005.
2. Kopecek J. Hydrogel biomaterials: a smart future? Biomaterials. 2007; 28:5185–92. [PubMed: 17697712]

3. Thiele J, Ma Y, Bruekers SMC, Ma S, Huck WTS. 25th Anniversary Article: Designer Hydrogels for Cell Cultures: A Materials Selection Guide. Advanced materials. 2013:125–148. [PubMed: 24227691]
4. Henderson KJ, Zhou TC, Otim KJ, Shull KR. Ionically Cross-Linked Triblock Copolymer Hydrogels with High Strength. Macromolecules. 2010; 43:6193–6201.
5. Gong J, Katsuyama Y, Kurokawa T, Osada Y. Double-Network Hydrogels with Extremely High Mechanical Strength. Advanced Materials. 2003; 15:1155–1158.
6. Sun JY, et al. Highly stretchable and tough hydrogels. Nature. 2012; 489:133–6. [PubMed: 22955625]
7. Hao J, Weiss R. Mechanical behavior of hybrid hydrogels composed of a physical and a chemical network. Polymer. 2013; 54:2174–2182.
8. Zhao X. Multi-scale multi-mechanism design of tough hydrogels: building dissipation into stretchy networks. Soft Matter. 2014; 10:672. [PubMed: 24834901]
9. Mozhdehi D, Ayala S, Cromwell OR, Guan Z. Self-Healing Multiphase Polymers via Dynamic Metal-Ligand Interactions. Journal of the American Chemical Society. 2014
10. Rubinstein, M.; Colby, RH. Polymer Physics. OUP; Oxford: 2003.
11. Holten-Andersen N, Fantner GE, Hohlbauch S, Waite JH, Zok FW. Protective coatings on extensible biofibres. Nature Materials. 2007; 6:669–72. [PubMed: 17618290]
12. Harrington MJ, Masic A, Holten-Andersen N, Waite JH, Fratzl P. Iron-clad fibers: a metal-based biological strategy for hard flexible coatings. Science (New York, NY). 2010; 328:216–20.
13. Yount WC, Juwarker H, Craig SL. Orthogonal control of dissociation dynamics relative to thermodynamics in a main-chain reversible polymer. Journal of the American Chemical Society. 2003; 125:15302–15303. [PubMed: 14664569]
14. Yount WC, Loveless DM, Craig SL. Strong means slow: dynamic contributions to the bulk mechanical properties of supramolecular networks. Angewandte Chemie (International ed in English). 2005; 44:2746–8. [PubMed: 15806606]
15. Fullenkamp DE, He L, Barrett DG, Burghardt WR, Messersmith PB. Mussel-Inspired Histidine-Based Transient Network Metal Coordination Hydrogels. Macromolecules. 2013; 46:1167–1174. [PubMed: 23441102]
16. Holten-Andersen N, et al. Metal-coordination: using one of nature's tricks to control soft material mechanics. Journal of Materials Chemistry B. 2014; 2:2467–2472.
17. Holten-Andersen N, et al. pH-induced metal-ligand cross-links inspired by mussel yield self-healing polymer networks with near-covalent elastic moduli. Proceedings of the National Academy of Sciences of the United States of America. 2011; 108:2651–2655. [PubMed: 21278337]
18. Lee H, Scherer NF, Messersmith PB. Single-molecule mechanics of mussel adhesion. Proceedings of the National Academy of Sciences of the United States of America. 2006; 103:12999–13003. [PubMed: 16920796]
19. Menyo MS, Hawker CJ, Waite JH. Versatile tuning of supramolecular hydrogels through metal complexation of oxidation-resistant catechol-inspired ligands. Soft Matter. 2013; 9:10314–10323.
20. Loveless DM, Jeon SL, Craig SL. Rational Control of Viscoelastic Properties in Multicomponent Associative Polymer Networks. Macromolecules. 2005; 38:10171–10177.
21. Yang CH, et al. Strengthening alginate/polyacrylamide hydrogels using various multivalent cations. ACS Applied Materials & Interfaces. 2013; 5:10418–22. [PubMed: 24128011]
22. Mckinnon DD, Domaille DW, Cha JN, Anseth KS. Biophysically Defined and Cytocompatible Covalently Adaptable Networks as Viscoelastic 3D Cell Culture Systems. Advanced Materials. 2014; 26:865–872. [PubMed: 24127293]
23. Rubinstein M, Semenov AN. Dynamics of entangled solutions of associating polymers. Macromolecules. 2001; 34:1058–1068.
24. Jongschaap RJJ, Wientjes RHW, Duits MHG, Mellema J. A Generalized Transient Network Model for Associative Polymer Networks. Macromolecules. 2001; 34:1031–1038.

25. Sing MK, Wang ZG, McKinley GH, Olsen BD. Celebrating Soft Matter's 10th Anniversary: Chain configuration and rate-dependent mechanical properties in transient networks. Soft matter. 2015; 00:1–12.

26. Ferry, JD. Viscoelastic Properties of Polymers. 3. Wiley & Sons, Inc; 1980.

27. Honerkamp J, Weese J. Determination of the relaxation spectrum by a regularization method. Macromolecules. 1989; 22:4372–4377.

28. Stadler FJ, Bailly C. A new method for the calculation of continuous relaxation spectra from dynamic-mechanical data. Rheologica Acta. 2008; 48:33–49.

29. McDougall I, Orbey N, Dealy JM. Inferring meaningful relaxation spectra from experimental data. Journal of Rheology. 2014; 58:779–797.

30. Sjöberg S. Critical evaluation of stability constants of metal-imidazole and metal-histamine systems. Tech Rep. 1997; 7

31. Annable T, Buscall R, Ettelaie R, Whittlestone D. The rheology of solutions of associating polymers: Comparison of experimental behavior with transient network theory. Journal of Rheology. 1993; 37:695.

32. Sever MJ, Wilker JJ. Visible absorption spectra of metal-catecholate and metal-tironate complexes. Dalton transactions. 2004:1061–72. [PubMed: 15252685]

33. Sakai T, et al. Design and Fabrication of a High-Strength Hydrogel with Ideally Homogeneous Network Structure from Tetrahedron-like Macromonomers. Macromolecules. 2008; 41:5379–5384.

34. Bae JE, Cho KS, Seo KH, Kang DG. Application of geometric algorithm of time-temperature superposition to linear viscoelasticity of rubber compounds. Korea-Australia Rheology Journal. 2011; 23:81–87.

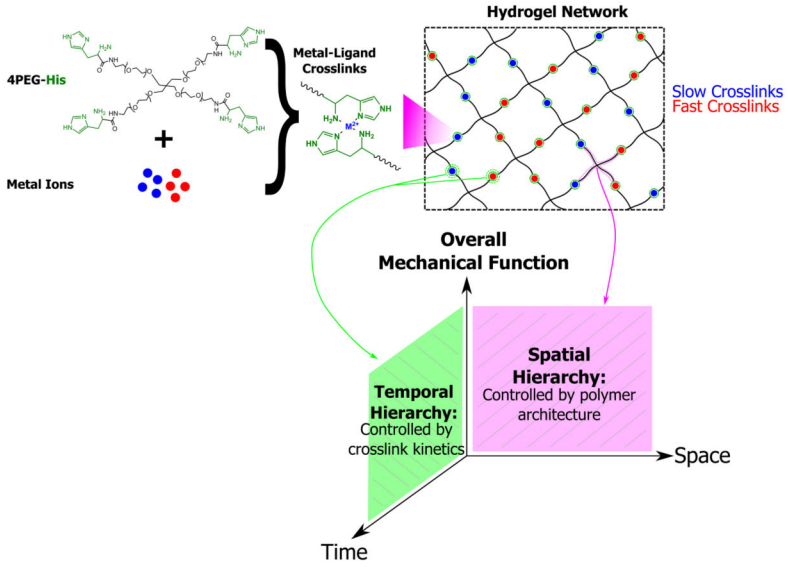

Figure 1. Model materials systems with orthogonally tunable mechanical temporal hierarchy

Model hydrogels with kinetically distinct crosslinks allow us to engineer the temporal hierarchy of the gel networks separately from the spatial hierarchy and thereby demonstrate a new conceptual framework for viscoelastic materials design. Spatial hierarchy represents a conventional strategy to engineer the viscoelastic properties of soft materials systems e.g. controlling material dynamics via polymer molecular structure. A material's temporal hierarchy can be controlled orthogonally from its spatial hierarchy by incorporating multiple metal-ligand crosslinks into single gel networks whereby material dynamics can instead be controlled by crosslink kinetics.

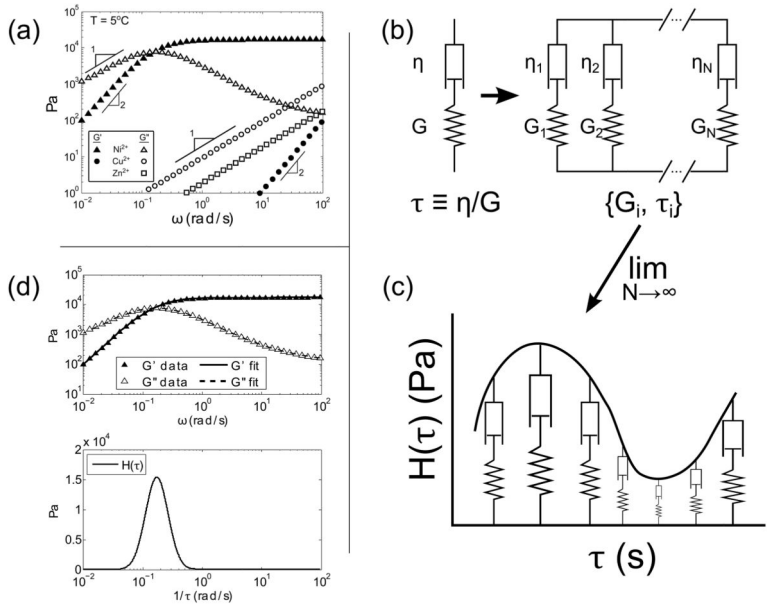

Figure 2. Rheological properties of single metal-ion hydrogels

(a) The inverse of the crossover frequency between $G'(\omega)$ and $G''(\omega)$ is called the relaxation time of the material, τ_c. A simple change of the metal ion in single metal-ion hydrogels can change this dissipative timescale by several orders of magnitude. At frequencies below the crossover, all gels show terminal relaxation mode-like behavior, where $G'(\omega) \sim \omega^2$ and $G''(\omega) \sim \omega^1$ as indicated. Extrapolation of the terminal relaxation behavior suggests $\tau_{Ni} > \tau_{Cu} > \tau_{Zn}$. Note that G'_{Zn} lies outside the range of these measurements and is therefore not shown. **(b)** A single Maxwell element, a spring with normalized spring stiffness G (units Pa) in series with a dashpot with normalized damping coefficient η (units Pa s). The characteristic relaxation time of the Maxwell element is given by the ratio $\tau = \eta/G$; a parallel series of N Maxwell elements can be described by a set of spring stiffnesses and relaxation times $\{G_i, \tau_i\}$ sometimes called the discrete relaxation spectrum; **(c)** in the limit where $N \to \infty$, the discrete set of parallel Maxwell elements becomes a continuous function, the relaxation spectrum $H(\tau)$.

(d) Single metal-ion gels (in this case His-Ni^{2+}) are well-characterized by a relaxation spectrum with a single dominant peak. The top part of the figure compares the experimental $G'(\omega)$ and $G''(\omega)$ data of the gel superimposed with the best-fit lines of $G'(\omega)$ and $G''(\omega)$ generated from fitting a two-mode relaxation spectrum $H(\tau)$ in the bottom part of the figure using Equations (1) and (2) (see Methods for further details on the fitting procedure). Note that $H(\tau)$ is shown as a function of $1/\tau$ for x-axes alignment.

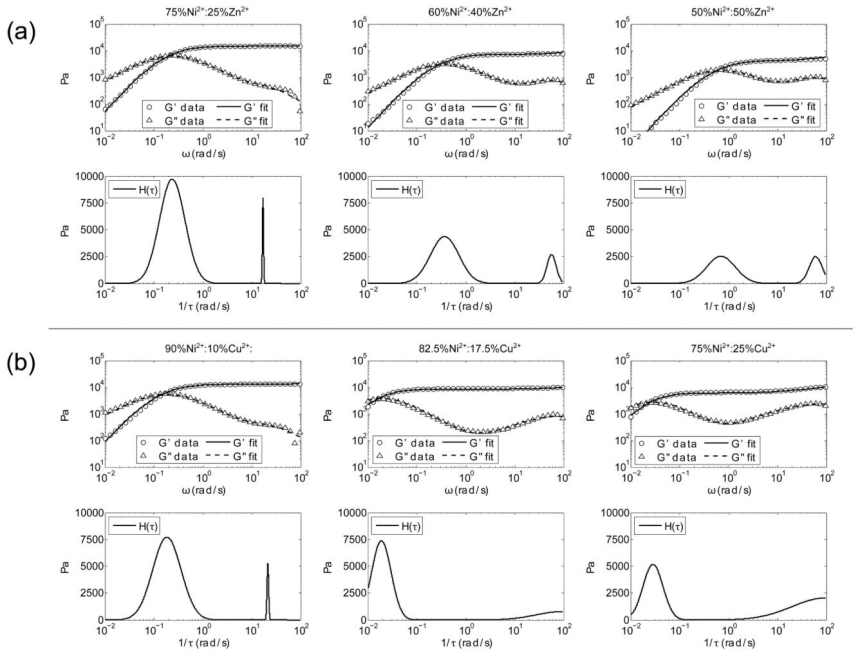

Figure 3. Hierarchical mechanics of double metal-ion coordinate networks

By varying the relative amounts of Ni^{2+} and **(a)** Zn^{2+} or **(b)** Cu^{2+} we can control the active crosslinks within the hybrid gel network and thereby modulate the relative magnitudes of their corresponding energy dissipation modes. The two local maxima in $G''(\omega)$ in each hybrid network are indicative of two distinct relaxation mode distributions, which we can fit to the relaxation spectra $H(\tau)$ as seen in the lower part of each figure. A double log-normal relaxation spectrum describes the measured mechanical data very accurately (solid and dashed lines in the top plot of each figure). This shows that the relative magnitudes of the energy dissipation modes can be controlled simply by changing the relative concentration of the particular metal ions within the network. All gels were made with a 10 kg/mol 4PEG-His polymer at 100 mg/mL in de-ionized H_2O, and 2:1 His:M^{2+} and NaOH:His stoichiometric ratios.

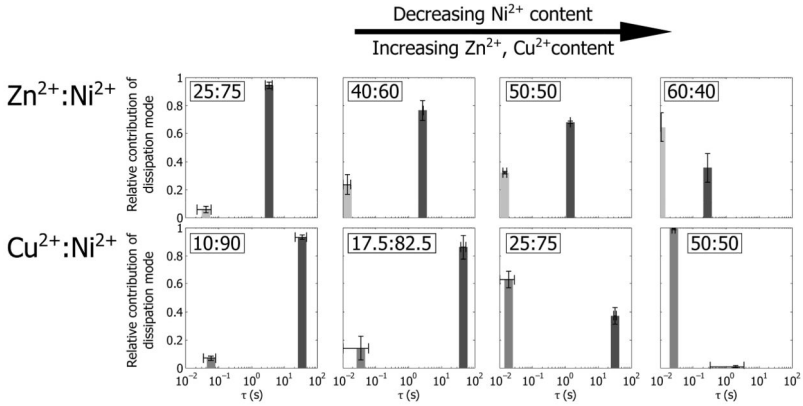

Figure 4. Relative contributions of slow and fast relaxation modes in double metal-ion hydrogels

When the total metal concentration is held constant, changing the ratios of Ni^{2+} ions (slow exchange kinetics) to Zn^{2+}/Cu^{2+} ions (fast exchange kinetics) directly modulates the relative contributions of the corresponding slow and fast dissipation modes (dark and light bars, respectively). (top) His- Zn^{2+}:Ni^{2+} gels and (bottom) His- Cu^{2+}:Ni^{2+} gels. Additionally, it is evident that Cu^{2+} and Zn^{2+} have differing abilities to modulate the time-dependent properties of the hydrogels; note especially that $\tau_{slow}(Cu^{2+}:Ni^{2+}) \gg \tau_{slow}(Zn^{2+}:Ni^{2+})$ and that $\tau_{slow}(Zn^{2+}:Ni^{2+})$ monotonically decreases with decreasing Ni^{2+} content. All error bars show the mean ± standard error, n = 2 except the His-10%Cu^{2+}:90%Ni^{2+} points where n = 4.

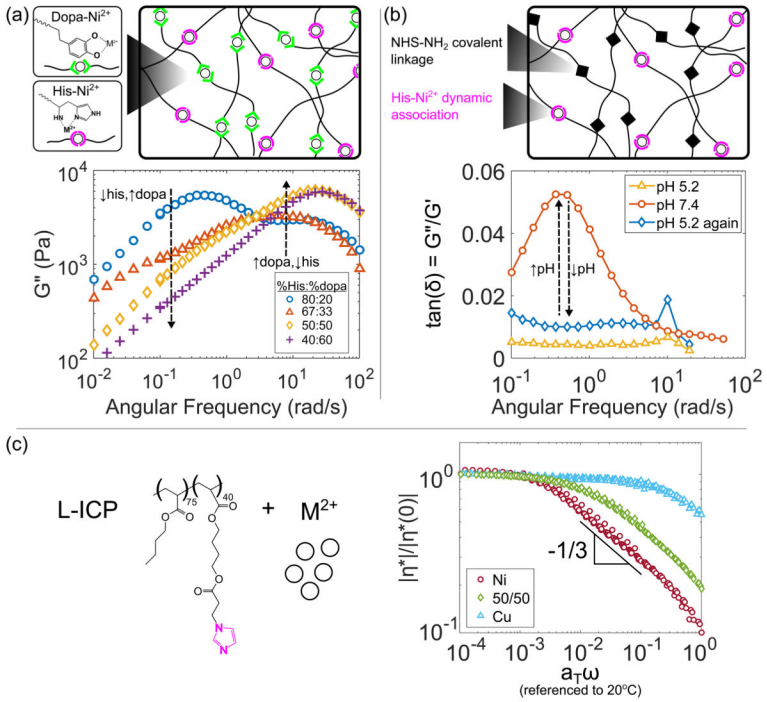

Figure 5. The effects of temporal mechanical hierarchy in systems beyond model 4PEG-His hydrogels

The effects of temporal hierarchy can be seen in different soft matter systems: **(a)** 4-arm PEG hydrogels crosslinked with both His-Ni^{2+} and dopa-Ni^{2+} show two characteristic timescales indicated by local maxima in G″. The contribution of the slow timescale ($\omega \sim 10^{-1} – 10^{0}$ rad/s) scales with the concentration of 4PEG-His, while the contribution of the fast timescale ($\omega \sim 10^{1} – 10^{2}$ rad/s) scales with the concentration of 4PEG-dopa. Hydrogels were made using the same procedure as those in Figures 2–4.

(b) Solid 4PEG hydrogels containing His-Ni^{2+} interactions show pH-responsive resonant energy dissipation, shown by the loss factor $tan(\delta)$. Physiologic pH triggers the formation of His-Ni^{2+} complexes, whose dynamic behavior results in resonant energy dissipation at a frequency $\omega \sim 10^{-1}–10^{0}$ rad/s. Lowering gel pH to 5.2 removes the resonance peak, demonstrating that pH-responsive energy dissipation can be induced in an otherwise permanent, elastic network.

(c) A random copolymer melt containing pendant imidazole moieties (L-ICP), mimicking histidine's metal-coordinating abilities, shows the generality of imidazole-metal coordination to control mechanical temporal hierarchy in an analogous yet different chemical environment. The normalized dynamic viscosities, $|\eta^*|/|\eta^*(0)|$ show that the terminal relaxation modes follow the order $\omega_{Ni} < \omega_{50/50} < \omega_{Cu}$, showing that histidine-like metal complexes can be used outside the hydrogel material space to engineer temporal mechanical hierarchy. Data shown are referenced to 20°C using time-temperature superposition from data taken at 20°C – 80°C.